



LAWRENCE
LIVERMORE
NATIONAL
LABORATORY

Contribution of Neutron Beta Decay to Radiation Belt Pumping from High Altitude Nuclear Explosions

R. E. Mars

November 13, 2002

This document was prepared as an account of work sponsored by an agency of the United States Government. Neither the United States Government nor the University of California nor any of their employees, makes any warranty, express or implied, or assumes any legal liability or responsibility for the accuracy, completeness, or usefulness of any information, apparatus, product, or process disclosed, or represents that its use would not infringe privately owned rights. Reference herein to any specific commercial product, process, or service by trade name, trademark, manufacturer, or otherwise, does not necessarily constitute or imply its endorsement, recommendation, or favoring by the United States Government or the University of California. The views and opinions of authors expressed herein do not necessarily state or reflect those of the United States Government or the University of California, and shall not be used for advertising or product endorsement purposes.

This work was performed under the auspices of the U.S. Department of Energy by University of California, Lawrence Livermore National Laboratory under Contract W-7405-Eng-48.

I. INTRODUCTION

In 1962, several satellites were lost following high altitude nuclear tests by the United States and the Soviet Union. These satellite failures were caused by energetic electrons injected into the earth's radiation belts from the beta decay of bomb produced fission fragments and neutrons. It has been 40 years since the last high altitude nuclear test; there are now many more satellites in orbit, and it is important to understand their vulnerability to radiation belt pumping from nuclear explosions at high altitude or in space. This report presents the results of a calculation of the contribution of neutron beta decay to artificial belt pumping.

For most high altitude nuclear explosions, neutrons are expected to make a smaller contribution than fission products to the total trapped electron inventory, and their contribution is usually neglected. However, the neutron contribution may dominate in cases where the fission product contribution is suppressed due to the altitude or geomagnetic latitude of the nuclear explosion, and for regions of the radiation belts with field lines far from the detonation point. In any case, an accurate model of belt pumping from high altitude nuclear explosions, and a self-consistent explanation of the 1962 data, require inclusion of the neutron contribution. One recent analysis of satellite measurements of electron flux from the 1962 tests found that a better fit to the data is obtained if the neutron contribution to the trapped electron inventory was larger than that of the fission products [1].

Belt pumping from high altitude nuclear explosions is a complicated process. Fission fragments are dispersed as part of the ionized bomb debris, which is constrained and guided by the earth's magnetic field. Those fission products that beta decay before being lost to the earth's atmosphere can contribute trapped energetic electrons to the earth's radiation belts. There has been a large effort to develop computer models for the contribution of fission products to belt pumping (e.g., the SNRTACS code system [2]). It is a daunting task because multiple, difficult-to-model plasma processes must be included, and existing belt pumping models cannot reproduce the trapped electron numbers, spectra, and spatial distributions observed following the 1962 tests.

Neutrons are not affected by the earth's magnetic field or by plasma electric and magnetic fields, so their contribution to belt pumping can in principle be calculated more accurately than that of fission products. Those neutrons emitted in an upward direction from a high altitude nuclear explosion travel in straight lines. They beta decay and contribute a trapped energetic electron to the earth's radiation belts at a rate determined by the 900-second neutron lifetime (which is much longer than the ~ 2 -second flight time of a fast neutron through the radiation belts). Neutrons emitted in a downward direction will scatter in the atmosphere. Most of them will diffuse out of the atmosphere and travel up through the earth's radiation belts, where their probability of injecting a trapped electron is now greater because of their lower velocity. This albedo effect increases the amount of belt pumping from neutron beta decay by several fold.

In the present work, we use Monte Carlo neutron transport techniques to account for the albedo effect of the earth's atmosphere and obtain accurate values for the magnitude and distribution of trapped electrons from neutron beta decay.

II. EARTH'S RADIATION BELTS

The earth's natural radiation belts consist of energetic charged particles (mostly electrons and protons) trapped in the earth's magnetic field. The region of closed magnetic field lines and stable trapping extends to roughly five earth radii from the center of the earth. The outer margin of the radiation belts is not well defined because of time varying distortions from the solar wind and interplanetary magnetic field. The inner margin of the radiation belts is determined by particle losses in the atmosphere and is much sharper. There is essentially no trapped radiation below 400 km altitude. There is a "slot" in the natural radiation belts in the neighborhood of 2.5 earth radii from the center of the earth where the flux of trapped particles is much lower than at higher or lower altitudes. The slot is attributed to resonant interactions between trapped particles and plasma waves that increase particle loss rates in this region. The natural radiation belts define the regions of stable trapping that can be pumped by nuclear explosions.

A. Earth's Magnetic Field

The earth's field is approximately that of a point dipole located near the center of the earth. Since trapped particles move along magnetic field lines, it is conventional to use the field lines to define toroidal magnetic shells or belts that encircle the earth. Magnetic shells are denoted by their "L-value," where L is defined as the distance of a magnetic field line from the center of the earth at the geomagnetic equator measured in earth radii ($r_e = 6371$ km). So the region of stable trapping extends approximately from $L = 1.02$ to $L = 5$.

For the present belt pumping calculations we use a point dipole approximation for the earth's magnetic field. The magnitude of the earth's field at the equator is then

$$B_0 = \frac{0.311}{L^3} \text{ Gauss.} \quad (1)$$

The equation of a dipole field line in polar coordinates is

$$r = r_0 \cos^2 \lambda \quad (2)$$

where r_0 is the distance from the center of the earth to the point at which the field line intersects the equatorial plane, and λ is the latitude. The magnetic field varies with position along a given field line according to

$$B(\lambda) = B_0 \frac{(4 - 3 \cos^2 \lambda)^{1/2}}{\cos^6 \lambda} \quad (3)$$

The point dipole approximation is good enough for an accurate calculation of the capture and motion of electrons from neutron beta decay. The most important deviations of the earth's field from that of a point dipole at the center of the earth, none of which have a significant effect on the initial capture of neutron decay electrons, are: (1) a slight offset (~ 400 km) of the dipole from the earth's center so that magnetic field lines are closest to the earth's surface over South America and the South Atlantic; (2) Time varying distortion of the field shape at large radius; and (3) a magnetic "bubble" at the detonation point of a nuclear explosion that persists for a few seconds.

B. Charged Particle Motion

The motion of a charged particle trapped in a dipole field has three components: a rapid cyclotron motion, a slower north-south bounce motion between mirror points on the same magnetic field line, and a much slower east-west drift as illustrated in Fig. 1. For energetic electrons trapped in the earth's field the gyroperiod is of order $4 \mu\text{s}$, the bounce period is of order 1 s, and the (eastward) drift time around the globe is of order 1 hr. Electrons have a gyroradius of a few hundred meters in the earth's field, depending on their energy and location.

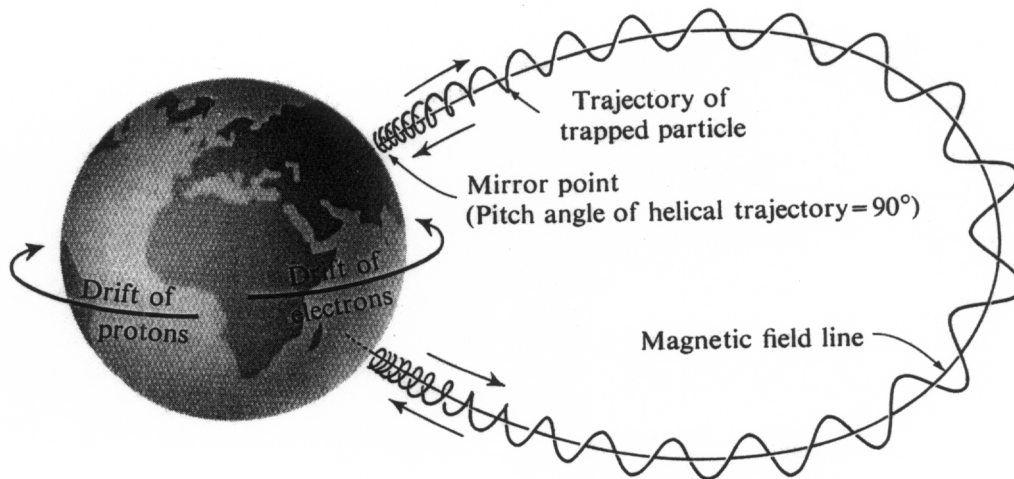


Fig. 1 Illustration of the motion of a charged particle trapped in the earth's magnetic field. (From Ref. 3)

The charged particle motion is characterized by a pitch angle α , which is the angle between the particle velocity vector and the local magnetic field direction. Conservation of angular momentum requires that $\sin^2 \alpha$ varies as B . A charged particle will have a mirror point (bounce) at a magnetic field for which $\alpha = 90$ degrees. Only those particles with mirror points above the earth's atmosphere will be trapped, so the restriction on pitch angles for trapped particles is

$$\sin^2 \alpha > \frac{B}{B_m} \quad (4)$$

where B is the local magnetic field and B_m is the maximum or mirror field on the same field line, (i.e., the field at the top of the earth's atmosphere). All particles with smaller pitch angle are in the "loss cone" and are not trapped. Although particles with different pitch angles mirror at different points, every trapped particle passes through the equator, where its pitch angle is largest, and it is useful to express the loss cone in terms of equatorial pitch angle:

$$\sin^2 \alpha_0 > \frac{B_0}{B_m} = \frac{1}{L^3 \left(4 - \frac{3}{L}\right)^{1/2}} \quad (5)$$

where the ratio of equatorial and mirror fields has been expressed in terms of L value. Note that the loss cone is independent of particle energy. As illustrated in Fig. 2, the loss cone is largest for field lines with small L value, and at high latitude along a given field line. Hence beta decays of either fission products or neutrons that occur at these locations have a smaller probability of yielding a trapped electron.

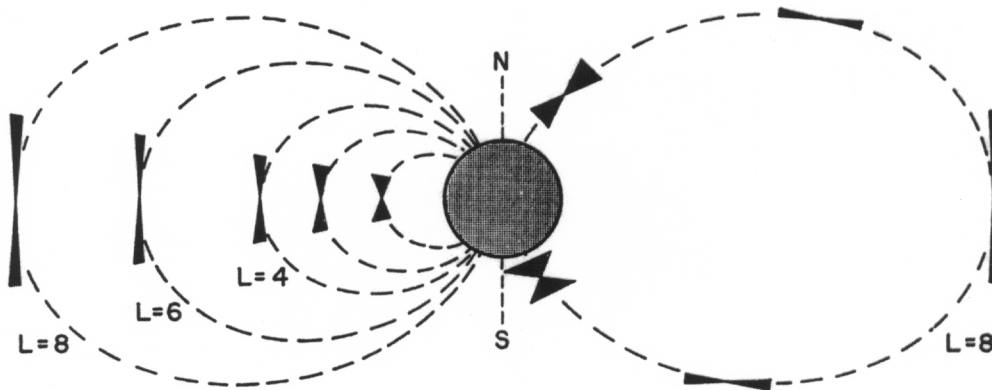


Fig. 2. Variation of loss cone size with L and with position along a magnetic field line of given L . (From Ref. 4)

III. ARTIFICIAL BELT PUMPING

Artificial belt pumping by nuclear explosions consists of energetic electrons from the beta decay of fission products and neutrons. Although the charged fission products and protons (from neutron beta decay) can also be trapped in the earth's magnetic field

and impact satellites, their range in solid material is much less than that of electrons and too low to damage satellites or register in the radiation detectors on satellites in 1962.

The spectrum of electrons from the beta decay of the neutron has an end point energy of 782 keV and is much softer than that of fission products. The neutron beta spectrum arises from a single transition and can be calculated exactly. Neglecting the small Coulomb correction factor, it has the form

$$\frac{dN}{d\varepsilon} \propto (\varepsilon_0 - \varepsilon)^2 \varepsilon \sqrt{\varepsilon^2 - 1} \quad (6)$$

where ε is the total relativistic electron energy (rest mass + kinetic) in units of mc^2 and ε_0 is the end point energy. The fission product beta spectrum is a composite of many transitions in different isotopes, and the spectrum also changes with time because the more energetic transitions tend to decay more rapidly. An effective fission product beta spectrum [5] is shown in Fig. 3 along with the neutron beta spectrum.

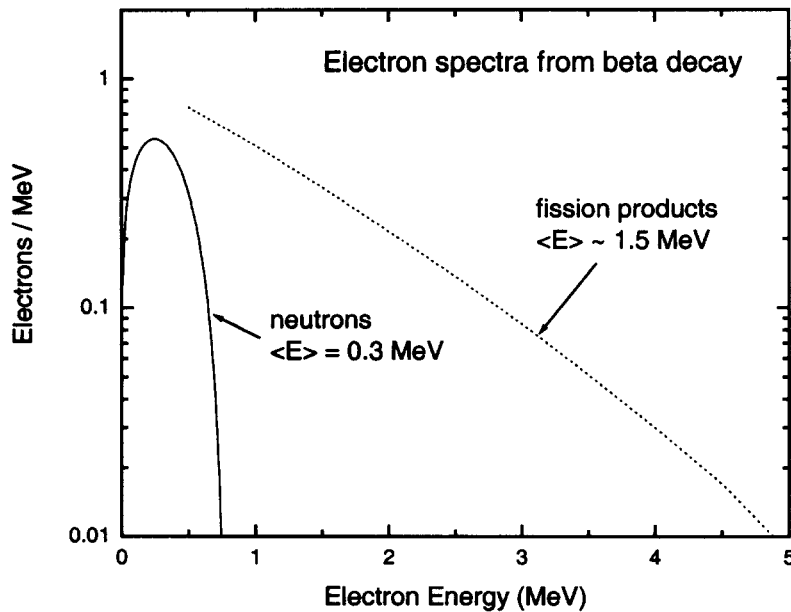


Fig. 3. Electron energy spectra for beta decay of the neutron and fission products. The average electron energies are 0.3 MeV for neutrons and 1.5 MeV for fission products.

The large difference between the electron spectra for neutron decay and fission product decay provides an opportunity to determine their separate contributions to belt pumping from spectral measurements of the trapped electron flux. Some spectral information is available for the 1962 high altitude tests. One of the best examples is shown in Fig. 4. These measurements are from a 5-channel magnetic spectrometer on an

air force polar orbiting satellite. They were obtained approximately 7.5 hours after a Russian test on 28 October 1962 and reflect belt pumping from that event. The different curves are for different L shells as labeled in the figure. As expected, the event created a hot spot within the natural belts at L values corresponding to the test location. The electron spectrum in the hot spot is close to that expected for fission product decay. At higher L values the spectrum appears to contain a softer component, which could be due to neutron decay. This is the expected behavior as the neutrons are not confined by the earth's magnetic field whereas the (charged) fission products are. Attempts to fit satellite data without including the neutron contribution could result in incorrect models of the belt pumping process. (Note that electron energies can be changed by the interaction of the bomb plasma with the earth's magnetic field, so the interpretation of measured energy spectra is not straightforward.)

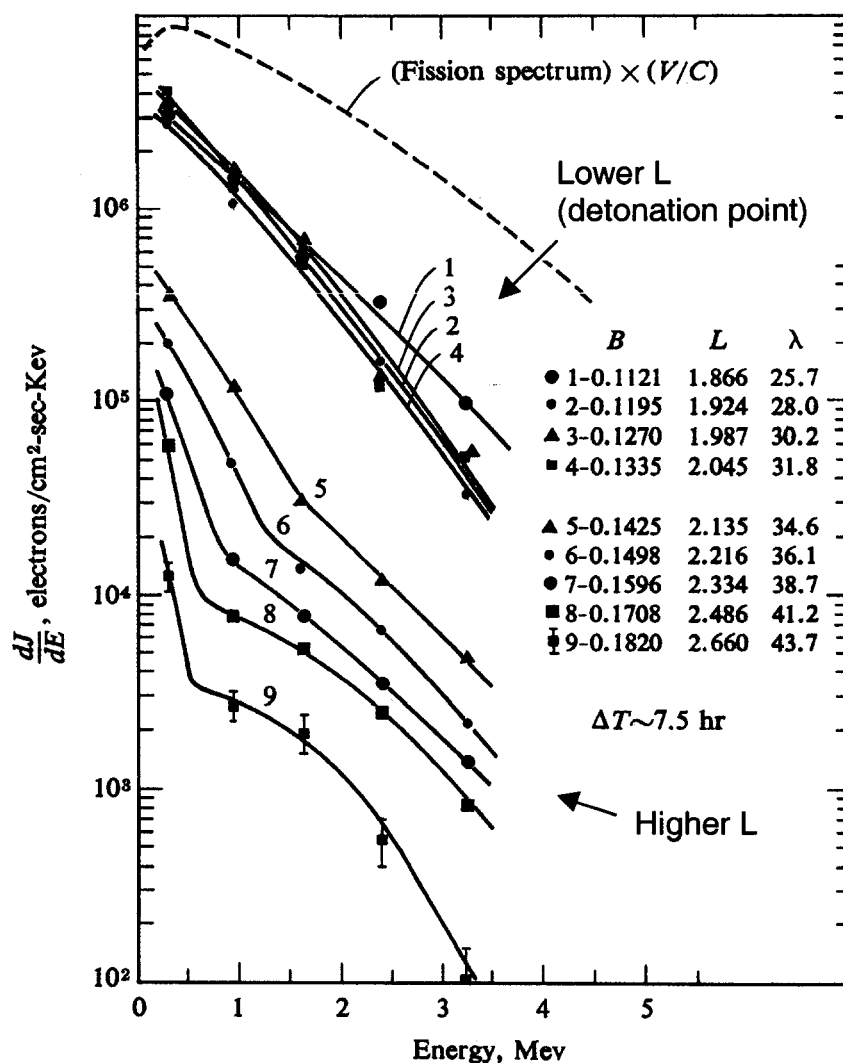


Fig. 4. Electron energy spectra following the Russian nuclear test of 28 October 1962 as measured by the Air Force β K satellite. (From Ref. 6)

The neutron output from a nuclear device depends on the design, but it is of order one neutron per fission, and each neutron emits a single beta. The two fission fragments from each fission together emit an average of approximately 5 betas before reaching stable nuclei. However neutrons have a much greater range than fission fragments in air or any other material and a greater chance to escape from a low altitude location where the electron trapping efficiency may be small. Hence the relative contribution of neutrons and fission products to belt pumping depends on the altitude of the nuclear explosion.

IV. MONTE CARLO CALCULATIONS

The contribution of neutrons to artificial belt pumping is dominated by albedo neutrons that backscatter from the atmosphere because these neutrons have a lower velocity and longer flight time through the radiation belts. Monte Carlo techniques provide the most accurate calculations of neutron scattering and diffusion. We used the MCNP Monte Carlo code [7] to calculate neutron transport from a nuclear explosive source, including neutron interactions in the atmosphere and their flight through the radiation belts. MCNP includes all important neutron interactions except for neutron decay, which we added as a separate factor. The region of space between the top of the earth's atmosphere and five earth radii was divided into 144 different "tally zones," and each tally zone was divided into 20 time bins, each with a separate decay factor. This makes it possible to obtain a distribution of neutron decay electrons over the different magnetic shells out to $L = 5$ as explained below.

Monte Carlo calculations are often used to obtain neutron flux at a particular location. However we do not need neutron flux, we need the average time that neutrons spend at a particular location or tally zone. This is a very different quantity. In fact, flux through a tally zone is proportional to neutron velocity whereas time in a tally zone is inversely proportional to velocity. MCNP includes an option to tally neutron path length divided by velocity in each tally zone, which is the time factor that we need for computing beta decay probability. The integrated neutron beta decay density in a spatial tally zone is then

$$N_{\beta} = \sum_{\substack{\text{neutron} \\ \text{histories}}} \left[\sum_{\substack{\text{time} \\ \text{bins}}} \langle R \rangle \left(\frac{l}{v} \right) \right] \quad (7)$$

where l is the neutron path length in the tally zone, v is the neutron velocity, and $\langle R \rangle$ is the average neutron decay rate within a time bin. The neutron decay rate falls exponentially with time according to

$$R = \frac{1}{\lambda_n} e^{-t/\lambda_n} \quad (8)$$

where λ_n is the neutron mean life of 886.7 seconds. MCNP tracks a very large number of neutron histories, sums their contributions, multiplies by the decay rate factors that we supply, and computes a time-integrated value for the beta decay density normalized to the number of source neutrons for each tally zone. A list of the time bins and decay rates used is given in Appendix I.

A. Effect of Neutron Source Energy and Altitude

We begin with a calculation of the effect of neutron source energy and altitude. Figure 5 shows the fraction of source neutrons that decay above the atmosphere and within five earth radii of the center of the earth (i.e., $1.02 < r/r_e < 5.0$) as a function of initial neutron energy. This is not exactly the same as the efficiency for pumping the radiation belts with $L < 5$ because we have not yet accounted for the loss of electrons with velocities inside the loss cone, and the large tally zone includes magnetic field lines at high latitude that correspond to $L > 5$. However the decay fraction is a good quantity for parameter studies. Figure 5 reveals the strong dependence of belt pumping efficiency on the initial energy of the neutrons: The belt pumping efficiency increases by approximately 100 fold from 1-MeV to 10-eV neutron energy, so the low energy tail of the neutron spectrum from a nuclear device is by far the most important for belt pumping.

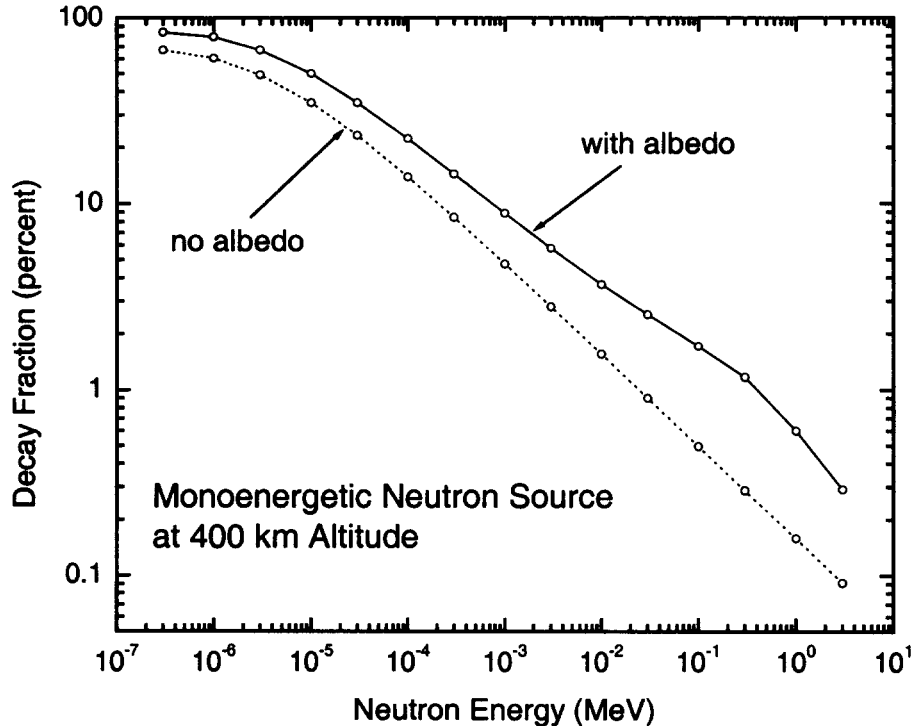


Fig. 5. Dependence of belt pumping efficiency on initial neutron energy. The curves show the fraction of source neutrons that decay within five earth radii from the center of the earth, with and without the effect of atmospheric albedo, as explained in the text. The circles are the calculated points.

The dashed curve in Fig. 5 shows the effect of removing the contribution of atmospheric albedo. This was done by making the earth's atmosphere a zone of complete absorption for neutrons. As can be seen in Fig. 5, atmospheric albedo increases the efficiency of belt pumping by a factor of 2 to 4, depending on the initial neutron energy.

The neutron source for the calculation of Fig. 5 was a point source emitting isotropically and located at an altitude of 400 km. This altitude is completely above the atmosphere but still close to the earth in units of earth radii. For a neutron source located at lower altitude, within the earth's upper atmosphere, there is an interesting dependence on altitude. As the amount of air overburden increases, the neutron belt pumping efficiency at first increases due to the increase in atmospheric scattering, and then decreases due to absorption. This is illustrated in Fig. 6, where the decay fraction within five earth radii is plotted as a function of air overburden. The maximum belt pumping efficiency occurs for an air overburden of 20 g/cm^2 , which corresponds to an altitude of about 30 km. For a nuclear explosion at this altitude the fission fragments and the betas they emit would be completely absorbed in the atmosphere and contribute nothing to belt pumping.

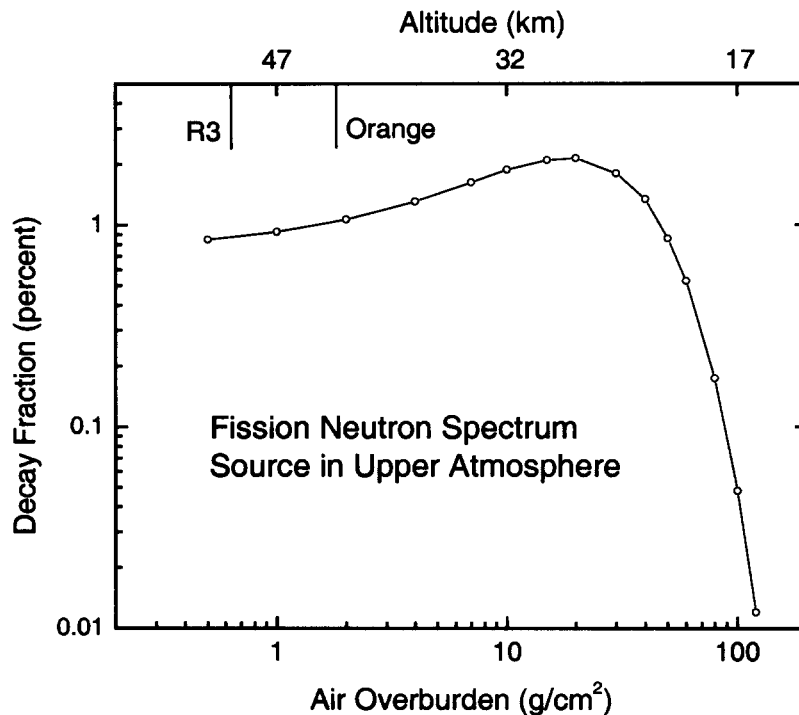


Fig. 6. Dependence of belt pumping efficiency on source altitude. The neutron decay fraction, as defined for Fig. 5, is plotted as a function of air overburden for a neutron source with a 1.23-MeV Maxwellian fission spectrum. Approximate values for equivalent altitude corresponding to 1, 10, and 100 g/cm^2 overburden are given along the top axis. Altitudes of the Orange and R3 tests are indicated.

A Maxwellian fission neutron spectrum of the form

$$p(E) = c\sqrt{E} e^{-E/a} \quad (9)$$

was used to calculate the effect of air overburden. Here c is a normalization constant and $a = 1.23$ MeV is a temperature. The average neutron energy is 1.93 MeV. When this source is located at 400-km altitude and compared with the monoenergetic source used for Fig. 5, the resulting decay fraction is almost exactly the same as that for 1.0-MeV monoenergetic neutrons.

The density gradient of the earth's atmosphere has essentially no effect on neutron transport. In other words, the belt pumping efficiency is the same for a constant density atmosphere with a sharp cutoff and for the actual exponential density profile. The only difference is a small effect due to slightly different neutron flight times because air mass is at different locations for different density profiles. We used an atmospheric density profile consisting of multiple constant density shells as listed in Table I. The thickness of the outer shell is 30 g/cm^2 (several neutron mean free paths), so very few neutrons penetrate to the other shells, whose density is therefore irrelevant for the Monte Carlo calculations. The air was assumed to be dry (no H_2O) with a composition of 78.1% nitrogen, 21% oxygen, and 0.9% argon by atomic percent; variations in composition with altitude were neglected.

Table I. Radius and air density for the shells in the MCNP atmosphere model.

Radius (km)	Air density (g/cm^2)
< 6371	earth
6371 - 6381	1.4×10^{-3}
6381 - 6391	3.0×10^{-4}
6391 - 6401	1.0×10^{-4}
6401 - 6411	3.0×10^{-5}
> 6411	0

B. L-Shell Distribution of Neutron Pumping

In this section we describe the calculation of the absolute magnitude of belt pumping from neutron beta decay and the distribution of the injected electrons over different L shells. In view of the fact that the easterly drift time for electrons around the earth is of order one hour, and the fact that neutron decays fill a large fraction of the radiation belt volume compared to fission product decays, we neglect the early time

dependence of belt pumping and average the results over longitude. This is the distribution that the electrons relax to after a few hours time. Taking advantage of the assumed azimuthal symmetry, we construct spatial tally zones that are annular rings encircling the earth.

Choice of tally zones

Ideally, we would divide the radiation belts into many bands of magnetic field lines (L shells), and subdivide each band into many individual latitude segments, each of which would be a tally zone. In the MCNP code it is difficult to use dipole field lines as boundary surfaces for tally zones, so we used spheres and cones as boundaries. We divided the region of space from $1.02 < r/r_e < 5.0$ into 12 different spherical shells, and subdivided each spherical shell into several rings by latitude. The tally zone construction is illustrated in Fig. 7, where two of the 144 zones used are shaded. Also shown in Fig. 7 are two magnetic field lines that define the L shell spanning the range $1.8 < L < 2.0$.

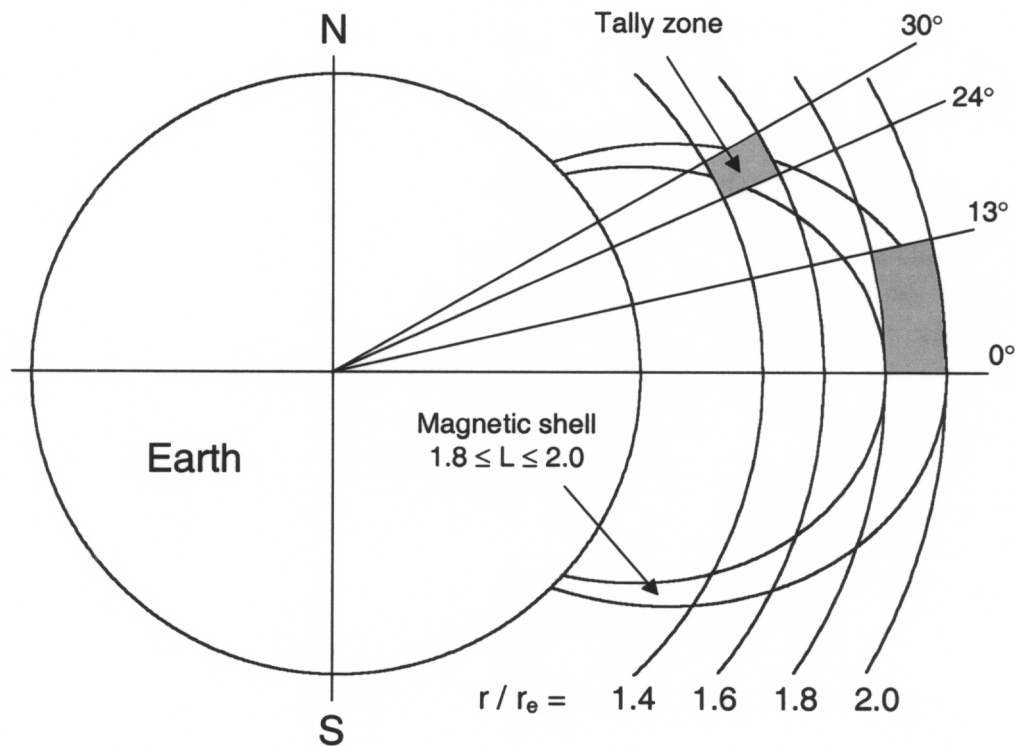


Fig. 7. Illustration of the MCNP tally zone geometry and its mapping onto L shells in the earth's radiation belts.

We chose 12 different L-shell bins, as listed in Table II, to determine how radiation belt pumping from neutron decay is distributed with respect to L value. Each L shell overlaps several different tally zones at different radius and latitude. Latitude zone

boundaries within each spherical shell were selected independently to give good overlap with the L-shell bins, and the tally results for each tally zone were assigned to the L shell with which the zone has the greatest overlap. For example, the neutron beta decays occurring in both of the shaded tally zones in Fig. 7 would be assigned to the 1.8 - 2.0 L shell.

Table II. L-shell bins used for calculating the distribution of belt pumping. The bins are labeled by the value of L in the center.

L range	Label
1.02 - 1.1	1.06
1.1 - 1.2	1.15
1.2 - 1.4	1.3
1.4 - 1.6	1.5
1.6 - 1.8	1.7
1.8 - 2.0	1.9
2.0 - 2.5	2.25
2.5 - 3.0	2.75
3.0 - 3.5	3.25
3.5 - 4.0	3.75
4.0 - 4.5	4.25
4.5 - 5.0	4.75

The output from the MCNP Monte Carlo calculation is a tally number for each zone that is proportional to the probability of neutron decay in that zone. Each of the zone tally numbers must then be multiplied by a loss cone factor to account for the fraction of decay electrons that are trapped. The trapping fraction is $\cos \alpha$, where α is the loss cone angle determined by the ratio of the local magnetic field and the mirror field at the top of the atmosphere along the same field line (see Eq. 4). We used a loss radius of 6500 km, corresponding to an altitude of 129 km, for computing the mirror field for each L shell. The local magnetic field was taken to be the field at the center of each tally zone. A list of all the tally zones and their properties is given in Appendix II.

Time dependence

Having defined tally zones within the radiation belts and a method for calculating the number of trapped neutron beta decay electrons for each zone, we are now ready to perform Monte Carlo calculations for the distribution of pumping within the radiation belts. Although we do not use the belt pumping rate in the present work, it is important

to know how this rate compares to other time scales in the problem. The pumping rate for a typical tally zone is shown in Fig. 8. The neutron source was a 1.23-MeV Maxwellian fission spectrum source located on the geomagnetic equator at 400 km altitude. Also shown in Fig. 8 is the neutron fluence in the same tally zone. As can be seen in the figure, more than 80% of the neutron fluence occurs before 1 s, but over half the belt pumping occurs after 100 s due to the inverse velocity weighting for neutron decay (see Eq. 7). This time is long compared to both the (~ 1 s) electron bounce time along magnetic field lines and the decay time for initial perturbations of the earth's magnetic field such as a magnetic bubble at the nuclear detonation point, which relaxes within a few seconds. Hence belt pumping from neutron beta decay is insensitive to perturbations of the earth's magnetic field caused by the nuclear detonation.

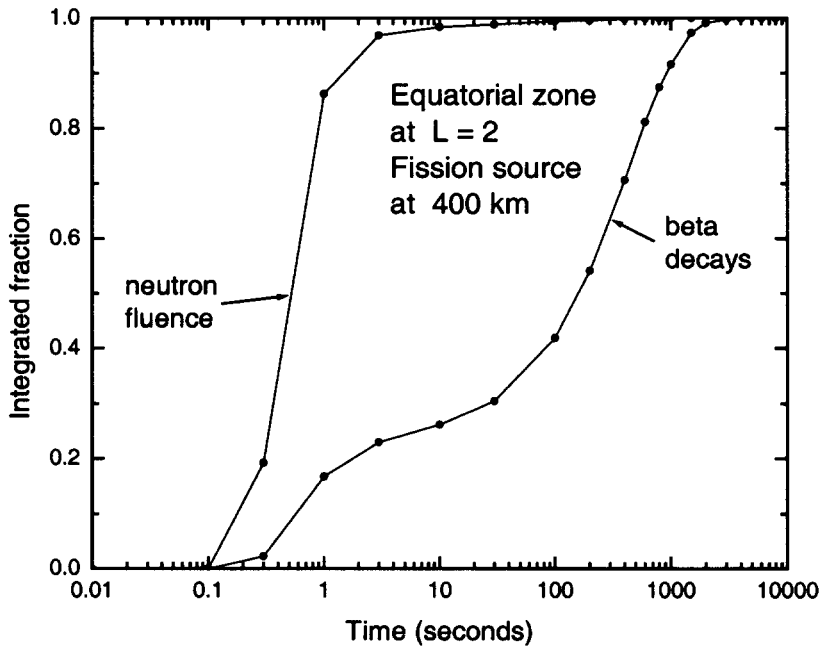


Fig. 8. Neutron fluence and beta decays in a tally zone at approximately 6400 km altitude ($L \approx 2$) on the geomagnetic equator. The circles are the calculated points.

Pitch angle relaxation

The distribution of trapped electrons from neutron beta decay is specified by density and pitch angle. (The electron energy distribution is a property of the neutron beta decay and is unchanged in a constant magnetic field.) Since every trapped electron passes through the geomagnetic equator, the electron distribution at every point along a magnetic field line is determined by the density and pitch angle distribution of electrons at the geomagnetic equator. Because of the conservation of canonical angular momentum, trapped electrons retain a "memory" of the magnetic field at their injection point. For example, if all electrons were injected near the ends of a magnetic field line

(i.e., at low altitude) where the field is strongest, then the pitch angle distribution at the geomagnetic equator would have a hole at large angles because electrons with equatorial pitch angles near 90 degrees can not reach the poles.

Pitch angle memory has a small effect on the pitch angle distribution of electrons from neutron beta decay because of the extended distribution of neutron decay points. Furthermore, the relaxation time for a nonuniform pitch angle distribution is a few days; so the electrons will have a normal mode distribution within a few days if not initially. For these reasons, we assume a relaxed pitch angle distribution for the present calculations. Relaxation means that available phase space is filled uniformly and the distribution of electrons within an L shell is completely characterized by one number, the total number of electrons in the shell or, equivalently, the electron flux at any point. This has implications for satellite measurements of belt pumping since, if the electron distribution is relaxed, a measurement of the electron flux at any point along a field line determines it everywhere. (For simplicity we are neglecting the fuzzy cutoff of the equatorial pitch angle distribution at the edge of the loss cone.)

For a relaxed electron distribution, the electron flux ϕ_e (particles/cm²/s) is isotropic everywhere except for a hole at angles within the loss cone. The electron flux density $d\phi_e/d\Omega$ is the same everywhere along a magnetic field line, but the flux is not. Particle fluxes in the radiation belts are frequently reported as "omnidirectional flux," which is defined as the flux averaged over 4π sr solid angle; we report our results as omnidirectional flux. The electron density and omnidirectional flux are largest at the geomagnetic equator (low B) and smallest at high latitude (high B).

Calculated electron flux

The number of electrons from neutron beta decay injected into one of the L-shell bins is the sum of the contributions from the individual MCNP tally zones assigned to that L shell. The number of electrons from the i th tally zone N_i is the product of the MCNP tally output, the loss cone factor $\cos \alpha_i$, and the number of source neutrons. The electron density at the geomagnetic equator is obtained by distributing the total number of electrons in an L shell in proportion to the available phase space volume at each location as required by a relaxed distribution. The omnidirectional flux is the product of the electron density and average electron velocity. We now have the two numbers of interest for each L shell bin: total number of electrons and omnidirectional electron flux at the geomagnetic equator.

The technique described above can be used to calculate the contribution of neutron beta decay to belt pumping from high altitude nuclear explosions at any location. Figure 9 shows the calculated electron flux for two representative nuclear explosions, both of which were located at an altitude of 400 km and had a yield of 1.45×10^{26} neutrons with a 1.23-MeV Maxwellian fission spectrum. (This corresponds to 1 Mt of fission yield with the assumption of one output neutron per fission.) One of the sources was located at the geomagnetic equator, which is the approximate latitude of the 1962 American high altitude tests, and the other source was located at a geomagnetic latitude

of 45 degrees, which is the approximate location of the 1962 Russian high altitude tests. At large L , the belt pumping is almost identical for the two source locations, but it differs significantly for $L < 1.5$ because those magnetic field lines are much closer to the equatorial source location. Because the higher L shells account for most of the volume of the radiation belts, the total electron inventory (shown on the figure) is almost the same for both source locations.

We are aware of only one previous calculation of belt pumping from neutron decay. That calculation, by Killeen, Hess, and Lingenfelter 40 years ago, was done analytically using multigroup diffusion theory to account for atmospheric albedo [8]. The analytic calculation predicted an electron fluence of slightly less than $10^7 \text{ cm}^{-2}\text{s}^{-1}$ near the explosion site for the Starfish event (see below), which is in agreement with the present results as shown in Fig. 9.

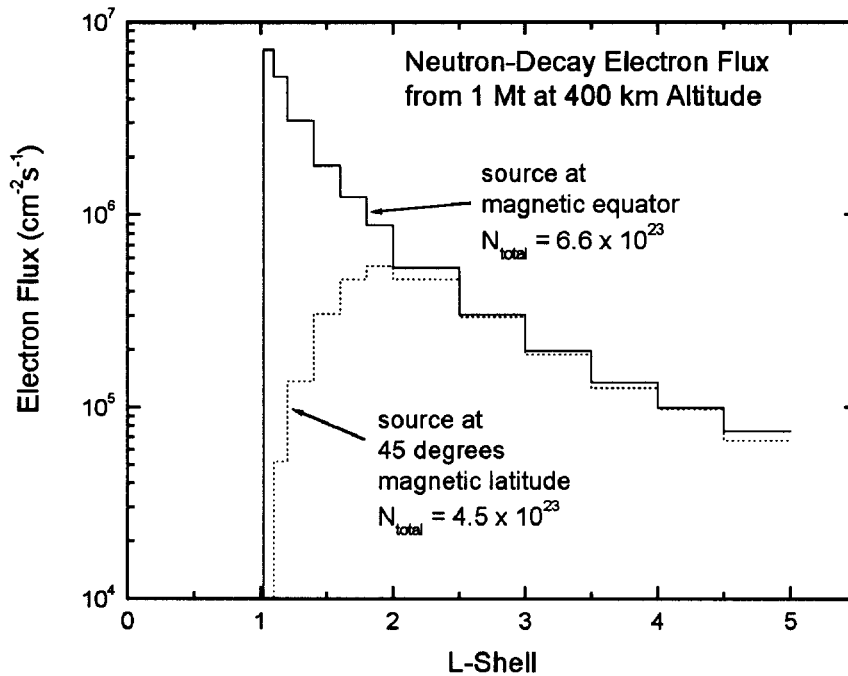


Fig. 9. Calculated electron flux in the radiation belts from neutron beta decay for a 1 Mt fission source at two different latitudes as labeled.

The density of protons injected into the radiation belts from neutron beta decay is the same as that of electrons. However the proton flux is roughly 100-fold less than the electron flux due to the lower proton velocity.

Production of neutrons in the earth's atmosphere by cosmic rays provides a natural source of belt pumping by neutron beta decay as these neutrons also diffuse out of the atmosphere and into space. The belt pumping rate from cosmic ray produced neutrons has been estimated at 10^{-13} to 10^{-12} electrons/cm³/s. For a radiation belt lifetime of 10^7 s (~100 days), which is typical for the largest volume of the belts, we expect an equilibrium electron density of order 10^{-6} to 10^{-5} electrons/cm³ for this natural source, neglecting the loss cone in the capture process. The corresponding electron flux is 10^4 to 10^5 electrons/cm²/s, well below the pumping level from a megaton high altitude nuclear explosion.

V. PAST HIGH ALTITUDE TESTS

There were six megaton-class high altitude tests conducted in 1958 and 1962 that should have injected neutron beta decay electrons into the radiation belts. The parameters of these tests are listed in Table III. The unclassified yields ranged from 0.3 to 1.4 Mt. The last column of the table lists values of the total electron inventory as inferred from satellite measurements of electron fluxes. There is a large uncertainty in the measured electron inventories as they can be obtained only with (possibly unrealistic) assumptions about electron spectra and distributions, and very different values are reported by different authors.

Table III. Past high altitude tests of importance for belt pumping. Total electron inventories are taken from: Teak and Orange (Ref. 9); Starfish, R1, R2, and R3, (Ref. 10).

event	date	yield	altitude (km)	latitude	detonation L-shell	total electron inventory
Teak	1 AUG 58	~Mt	77	17° N	1.1	$< 10^{21}$
Orange	12 AUG 58	~Mt	43	17° N	1.1	$< 10^{21}$
Starfish	9 JUL 62	1.4 Mt	400	17° N	1.12	1.3×10^{25}
R1	22 OCT 62	0.3 Mt	300	~48° N	1.9	3.6×10^{25}
R2	28 OCT 62	0.3 Mt	150	~48° N	2.0	1.2×10^{25}
R3	1 NOV 62	0.3 Mt	50	~48° N	1.8	1.2×10^{24}

A recent analysis by Allen and McDaniel [1] attempted to fit the 1962 test data, for which some electron spectral information is available, with a two-spectrum model -- one spectrum for neutron decay and the other for fission product decay (see Fig. 3). For each of the tests they determined separate values for the total electron inventory due to neutron decay and fission product decay. Their best-fit value for the neutron contribution was roughly 1.8×10^{26} electrons for Starfish, R1, and R2, and 1.5×10^{25} for R3. The higher value is comparable to the number of neutrons emitted by each of the devices, and

if correct would imply an unrealistic belt pumping efficiency of order 100% for neutron beta decay. The value for the total electron inventory from neutron decay calculated in the present work is roughly 5×10^{23} electrons for these four events if the neutrons have a 1.23-MeV Maxwellian fission spectrum. In addition to providing a value for neutron decay pumping, the two spectrum fit also significantly changes the amount of fission product pumping compared to a single spectrum model.

Whatever the size of the neutron contribution to the total electron inventory, the 1962 tests show a strong population of electrons at energies above the neutron beta decay end point and localized at L shells corresponding to the event location as expected from fission product decay. For example, pumping of the belts at $L = 1.2$ at the equator by Starfish was $\sim 1.5 \times 10^9$ electrons/cm²/s. However, the Teak and Orange events in 1958 produced little if any belt pumping from fission product decay, probably because of the low altitude and low latitude of these tests. Referring to Fig. 6, the altitude of Teak and Orange is still well above the altitude at which the neutron contribution to belt pumping is reduced by air overburden. Unfortunately, there were very few satellites in orbit in 1958 and none of them had radiation detectors with thresholds low enough to see the neutron decay electrons. If such detectors had been in place, they would have seen the neutron-decay belt pumping from these two events. Changes in radio wave propagation were observed in the United States for times of order 10 to 100 seconds following Teak and Orange, and this has been attributed to atmospheric ionization (above the U. S.) by electrons (in the loss cone) from beta decay of bomb produced neutrons [11].

Because of the strong dependence of belt pumping efficiency on initial neutron energy (see Fig. 5), neutron belt pumping would be much greater if a fraction of the source neutrons were thermalized in the bomb debris and came out with a lower energy. For example a 10-eV neutron is 100-fold more effective at belt pumping than a 1-MeV neutron. The present work can be combined with modern calculations of (low energy) neutron output from actual nuclear devices to obtain more accurate values of radiation belt pumping from neutron beta decay, which may be significantly larger than the values reported here.

VI. CONCLUSIONS

The beta decay of neutrons from high altitude nuclear explosions pumps the earth's radiation belts with energetic electrons that are spread throughout the stable trapping region of the belts. This is in contrast to belt pumping from fission product decay, which is concentrated in L shells at or near the detonation. Unless the contribution of fission products is suppressed because of the altitude or location of the explosion, it will certainly dominate the belt pumping for these L shells. In addition, the lower energy of the neutron beta decay spectrum makes these electrons less threatening to satellites than those from fission product decay. However an accurate model of artificial belt pumping must include the neutron contribution or there will be inconsistencies that lead to incorrect values for the fission product contribution. If the magnitude or L-shell distribution of belt pumping is modeled incorrectly, then the radiation dose to satellites could be substantially different than expected. Allen et al.

estimate that the existing model (SNRTACS) for satellite radiation dose from high altitude nuclear explosions may be in error by factors of 10 - 100 [1].

Even though no more high altitude nuclear tests are expected, poor models of weapon effects have immediate consequences. An incorrect understanding of the distribution and magnitude of belt pumping could lead to an incorrect choice of a possible future nuclear warhead for national missile defense or a misguided response to the threat of a hostile high altitude nuclear explosion.

If high altitude nuclear explosions occur in the future, then the energy resolution of radiation detectors now in space will easily separate the contributions to belt pumping from neutrons and fission products. Although the fission product contribution is difficult to model because of its complexity, the Monte Carlo method reported here provides a very accurate calculation of the neutron contribution and therefore a way to obtain information on the yield and neutron spectrum from any future high altitude nuclear event.

APPENDIX I: DECAY RATE FACTOR

The tallies for each time bin in the MCNP Monte Carlo calculations were multiplied by a rate factor that accounted for the loss from previous neutron decays and the average rate at which neutron decays occur during that time interval. The expression for the rate factor is

$$\langle R \rangle = \frac{1}{t_2 - t_1} (e^{-t_1/\lambda_n} - e^{-t_2/\lambda_n}) \quad (\text{A1})$$

where t_1 and t_2 are the beginning and end times for the time bin, and λ_n is the neutron lifetime of 886.7 s.

Table A1. Time bins and neutron decay rate factors used in the Monte Carlo calculations

Time interval (s)	$\langle R \rangle$ (s ⁻¹)
0 - 0.01	1.13×10^{-3}
0.01 - 0.1	1.13×10^{-3}
0.1 - 0.3	1.13×10^{-3}
0.3 - 1.0	1.13×10^{-3}
1.0 - 3.0	1.13×10^{-3}
3.0 - 10	1.12×10^{-3}
10 - 30	1.10×10^{-3}
30 - 100	1.05×10^{-3}
100 - 200	9.53×10^{-4}
200 - 400	8.06×10^{-4}
400 - 600	6.43×10^{-4}
600 - 800	5.13×10^{-4}
800 - 1000	4.10×10^{-4}
1000 - 1500	2.79×10^{-4}
1500 - 2000	1.59×10^{-4}
2000 - 3000	7.1×10^{-5}
3000 - 4000	2.3×10^{-5}
4000 - 6000	4.9×10^{-6}
6000 - 8000	5.2×10^{-7}
8000 - 10,000	5.4×10^{-8}

APPENDIX II: MONTE CARLO TALLY ZONES

Twelve spherical shells were divided into a total of 144 different tally zones using independent angular bins in each shell. Conical surfaces defined the angular range of each zone as shown in Fig. 7. The apex of each cone was located at the center of the earth, and the cone half angle is the (magnetic) latitude. The radial and angular boundaries and other properties of the tally zones are listed in Table A2. The zoning is symmetric between the northern and southern hemispheres.

Table A2. Monte Carlo tally zones. Entries are grouped by spherical shell radius and listed by range of latitude angle within each group. B is the magnitude of the earth's magnetic field at the center of the zone and α is the loss cone angle as defined in the text. Only the northern hemisphere tally zones are listed. The southern hemisphere tally zones are identical. The second column gives the L shell to which the beta decay tally from that zone contributes.

Angular range (degrees)	L-shell assignment	B (mG)	α (degrees)	Volume (10^{25} cm ³)
1st spherical shell $1.02 < r/r_e < 1.1$				
0 - 11	1.06	264	67.0	2.78
11 - 20	1.15	288	67.7	2.20
20 - 30	1.3	324	68.5	2.30
30 - 36	1.5	359	69.2	1.28
36 - 40	1.7	382	69.5	0.801
40 - 43	1.9	397	69.7	0.571
43 - 49	2.25	417	69.9	1.06
49 - 54	2.75	440	70.2	0.792
54 - 57	3.25	455	70.3	0.431
57 - 59	3.75	464	70.4	0.271
2nd spherical shell $1.1 < r/r_e < 1.2$				
0 - 12	1.15	208	51.2	4.47
12 - 25	1.3	233	52.5	4.62
25 - 32	1.5	265	53.7	2.31
32 - 37	1.7	286	54.4	1.55
37 - 41	1.9	302	54.8	1.17
41 - 47	2.25	320	55.2	1.62
47 - 52	2.75	338	55.6	1.22
52 - 55	3.25	351	55.8	0.669
55 - 58	3.75	359	56.0	0.623

3rd spherical shell $1.2 < r/r_e < 1.4$

0 - 16	1.3	146	38.2	15.17
16 - 26	1.5	167	39.7	8.95
26 - 32	1.7	185	40.7	5.04
32 - 36	1.9	197	41.3	3.19
36 - 44	2.25	212	42.0	5.88
44 - 49	2.75	227	42.5	3.30
49 - 52	3.25	236	42.8	1.84
52 - 55	3.75	243	43.0	1.71
55 - 58	4.25	249	43.2	1.59

4th spherical shell $1.4 < r/r_e < 1.6$

0 - 15	1.5	94.5	28.6	18.96
15 - 24	1.7	106	29.7	10.84
24 - 30	1.9	117	30.6	6.83
30 - 39	2.25	129	31.5	9.48
39 - 45	2.75	141	32.2	5.70
45 - 49	3.25	149	32.6	3.48
49 - 52	3.75	154	32.9	2.45
52 - 55	4.25	158	33.1	2.28

5th spherical shell $1.6 < r/r_e < 1.8$

0 - 14	1.7	64.7	22.6	22.74
14 - 23	1.9	72.2	23.6	13.99
23 - 35	2.25	82.7	24.7	17.19
35 - 41	2.75	92.5	25.6	7.76
41 - 46	3.25	98.5	26.0	5.94
46 - 49	3.75	103	26.3	3.33
49 - 52	4.25	106	26.5	3.15
52 - 54	4.75	108	26.7	1.96

6th spherical shell $1.8 < r/r_e < 2.0$

0 - 13	1.9	46.2	18.6	26.41
13 - 29	2.25	53.4	19.7	30.50
29 - 37	2.75	62.3	20.8	13.74
37 - 43	3.25	67.9	21.4	9.41
43 - 46	3.75	71.3	21.7	4.37
46 - 49	4.25	73.5	21.9	4.15
49 - 52	4.75	75.7	22.1	3.93

7th spherical shell $2.0 < r/r_e < 2.5$

0 - 19	2.25	28.4	14.1	134.5
19- 30	2.75	33.6	15.1	72.05
30 - 37	3.25	37.8	15.8	42.06
37 - 41	3.75	40.4	16.1	22.42
41 - 45	4.25	42.3	16.4	21.07
45 - 48	4.75	43.8	16.6	14.86

8th spherical shell $2.5 < r/r_e < 3.0$

0 - 17	2.75	15.4	10.1	180.1
17- 28	3.25	17.9	10.8	109.1
28 - 34	3.75	20.0	11.3	55.3
34 - 39	4.25	21.5	11.6	43.2
39 - 42	4.75	22.5	11.8	24.6

9th spherical shell $3.0 < r/r_e < 3.5$

0 - 16	3.25	9.32	7.7	237.1
16- 26	3.75	10.66	8.2	139.9
26 - 32	4.25	11.83	8.6	78.7
32 - 36	4.75	12.61	8.8	49.8

10th spherical shell $3.5 < r/r_e < 4.0$

0 - 15	3.75	6.05	6.2	296.1
15- 24	4.25	6.81	6.5	169.2
24 - 30	4.75	7.50	6.8	106.7

11th spherical shell $4.0 < r/r_e < 4.5$

0 - 14	4.25	4.14	5.1	355.4
14 - 23	4.75	4.62	5.3	218.7

10th spherical shell $4.5 < r/r_e < 5.0$

0 - 13	4.75	2.96	4.3	412.7
--------	------	------	-----	-------

References

1. "Review of the High Altitude Nuclear Burst 1958 and 1962 Satellite Data," C. Allen and P. McDaniel (unpublished); C. Allen, private communication.
2. "Development of Multi-Burst Electron Radiation Belt Injection, Loss and Redistribution Model," J. B. Cladis, G. T. Davidson, and W. E. Francis, PL-TR-92-1078, June, 1993.
3. *The Radiation Belt and Magnetosphere*, W. N. Hess, Blaisdell, 1968.
4. "Precipitation of Electrons and Protons into the Atmosphere," B. J. O'Brien in *Radiation Trapped in the Earth's Magnetic Field*, B. M. McCormac ed., Gordon and Breach, 1966.
5. "Electron Antineutrino Spectrum for $^{235}\text{U}(n,f)$," J. K. Dickens, Phys. Rev. Lett. **46**, 1061 (1981).
6. "Some Observations of the Trapped Electrons Produced by the Russian High Altitude Detonation of October 28, 1962," H. I. West in *Radiation Trapped in the Earth's Magnetic Field*, B. M. McCormac ed., Gordon and Breach, 1966.
7. *MCNP4B: A General Monte Carlo N-Particle Transport Code*, J. F. Briesmeister, Editor, LA-12625-M, March, 1997.
8. "Electrons from Bomb Neutron Decay," J. Killeen, W. N. Hess, and R. E. Lingenfelter, J. Geophys. Res. **68**, 4637 (1963).
9. "Artificial Injection of Electrons into the Geomagnetic Field by Teak and Orange, Low Altitude Bursts of 1958," D. J. Manson et al., J. Geophys. Res. **75**, 4710 (1970).
10. *The Trapped Radiation Handbook*, J. B. Cladis, G. T. Davidson, and L. L. Newkirk, Editors, DNA 2524H, November, 1973.
11. "A Note on the Cause of Sudden Ionization Anomalies in Regions Remote from High Altitude Nuclear Bursts," C. M. Crain and P. Tamarkin, J. Geophys. Res. **66**, 35 (1961).

Distribution

LLNL

Barish, Frank L-183
Bennett, Charlie L-183
Carman, Scott L-031
Carter, Mike L-183
Conaway, Bill L-183
Davis, Jay L-189
DiPeso, Greg L-183
Farley, Ed L-183
Gerassimenko, Mike L-183
Goodwin, Bruce L-160
Handler, Frank L-183
Hartouni, Ed L-056
Hewett, Dennis L-039
Hills, Rob L-181
Hoover, Todd L-015
Johnson, Kent L-160
Keller, Leon L-096
Kruger, Hans L-183
Larson, David L-039
Marrs, Ross L-183
Miller, Mike L-183
Nakafuji, Glen L-183
O'Brien, Hank L-160
Pomykal, Glenn L-183
Pruneda, Jenni L-180
Ramos, Tom L-182
Rowley, Dana L-097
Shaeffer, Lynn L-183
Simons, David L-180
Simonson, Greg L-180
Speed, Roger L-183
Spriggs, Greg L-030
Thomson, Tom L-015
Turano, Ed L-015
Tyler, Jim L-160
Volpe, Alan L-016
Ward, Richard L-013
Woodworth, John L-180

LANL

Winske, Dan X-1

SNL/NM

Griffin, Pat MS-1146

DOE/HQ

Luera, Ted NA-113.1

Allen, Charles
Logicon
Albuquerque, NM

McDaniel, Patrick
Air Force Research Laboratory
Albuquerque, NM